



Euler's equation grinding track, microgrinding mechanism, and process research of space optical crystal materials

Jiabin Xu¹ · Qiongyi He² · Xiangyu Zhang³ · Yang Yu² · Dongyu Tian¹ · Yingjie Li⁴ · Feihu Zhang¹

Received: 22 March 2023 / Accepted: 19 August 2023 / Published online: 6 September 2023
© The Author(s), under exclusive licence to Springer-Verlag London Ltd., part of Springer Nature 2023

Abstract

In microdiameter precision grinding of the YAG ($Y_3Al_5O_{12}$) optical crystal material, centerless precision grinding is the necessary process of the preparation method to obtain surface finish. To further obtain the optical crystal devices in optical field, the tiny diameter of the optical crystal material is the key element. However, the process to generate the grinding ratio of the grinding a_p forms part of precise control of the actual mathematical calculation for the ceramic base grinding wheel. In this work, we propose a satisfying precision grinding models for engineering applications and a theory to explain the grinding process of the microdiameter YAG optical crystal materials. A ceramic base of the grinding wheel axis is designed, and the wheel axis experimental parameters are regulated from controllable clearance and eccentricity for the e by the grinding depth and surface finish quality. The resultant parameters keep constant during the precision grinding and self-adaption dressing process to avoid the deviation caused by centrifugal force. In the process of self-adaption dressing of ceramic base grinding, wheel rotation direction is controlled by critical parameters such as the grinding wheel axis (-), and the regulating wheel axis (-) is the critical parameters to determine the final appearance of the grinding wheel. The value range of the feed location region is [0.022, 1.007]. Grinding wheel axis speed and regulating wheel axis speed are 35–60 RPM. Thus, the process challenges and technical issues of YAG optical crystal material microdiameter precision grinding can be solved.

Keywords Precision grinding process · Optical crystal materials · Grinding ratio · Direction of rotation

Highlights

- (1) The work illustrates the selection of an appropriate and optimal self-adaption dressing process for the grinding wheel parameters, which are of significance to the finish surface quality, cylindricity, and parallelism of the ceramic base grinding wheel in precision grinding.
- (2) The feasibility of self-adaption-dressing process for centerless grinding is verified. To improve the finish surface quality, roundness and parallelism of the YAG optical crystal are established in the geometric mathematical model which is then tested in verification.
- (3) A 3D (three-dimensional) analytical model and precision process for the precise centerless grinding of YAG crystal material is established. Grinding gap geometry and precision grinding process parameters based on real-time adjustment are designed and tested.

Jiabin Xu and Qiongyi He contributed equally to this work and should be considered co-first authors.

✉ Yingjie Li
lyjmx@163.com

✉ Feihu Zhang
zhangfh@hit.edu.cn

Extended author information available on the last page of the article

Abbreviations

a_p	Precision grinding depth, mm
Δa_p	Dynamic change of depth of grinding, mm
e	The precision grinding center of the eccentricity, mm
e_s	The precision grinding ratio, N/mm^2
D	Diameter of the YAG optical crystal material, mm
D_{YAG}	The diameter of the YAG optical crystal, mm
F	Tangential grinding force, N/mm^2
F_i	Grinding force per unit area, N/mm^2
F_n	The normal grinding force, N/mm^2
$N_{dividing}$	The number of teeth of indexing dial, Numbers
P_{screw}	The pitch of the feed direction, $\mu m/s$

Δ_t	Rotation interval time, min
$V_{\text{grinding wheel}}, V_{\text{regulating wheel}}$	The speed ratio, $\mu\text{m/s}$
W_{YAG}	The angular angle of the YAG optical crystal, deg
Ψ	The real grinding wheel radian direction of the ceramic base grinding wheel, + or -
Ψ_i	Rotation angle, deg
Ω_s	Constant speed, m/s
θ	Rotating angle of the ceramic base grinding wheel, deg
α	Ceramic base grinding wheel center angle, deg
β	Ceramic base grinding wheel center angle, deg

1 Introduction

Improving the optical properties of the optical materials by using ceramic-based grinding wheel and centerless grinding process is one of the practical engineering methods to solve the issues of microdiameter precision grinding of YAG ($\text{Y}_3\text{Al}_5\text{O}_{12}$) optical crystal materials. YAG is a new substrate and UV and infrared optical window materials, whose superior optical crystal properties are especially used in high-temperature and high-energy fields. The application of the precision grinding process is important to improve the surface finish, cylindricity and parallelism of the YAG difficult-to-grinding optical raw materials by centerless grinding process in optics and optical fields. However, issues such as grinding ratio and microscale of the grinding wheel still exist which affect the grinding process.

In 2004, Hashimoto et al. [1] proposed a steady-state rule, stating that the three indexes that affect stability are dynamic, geometric, and rotational. The influence of these grinding forces on the stability of high-speed rotation was analyzed [2]. Based on the N. Chiu & S. Malkin theoretical model and micro-grinding achieved on the 4-mm thick 0.8% YAG optical materials [3, 4].

Barrenetxea et al. [5, 6] revealed the importance of optimal parameter selection for variable speed precision grinding processes. After objective calculation and analysis, many researchers have obtained one of the changes in velocity over a short period of time. But this design and process method may lead to overload tiny diameter of the precision grinding ratio.

During the last twenty years, with the development of the optical crystal material preparation process, more factors of the optical resonator conditions have been taken into consideration during the grinding processes, including the grinding beating the grinding depth of a_p and grinding surface finish accuracy. However, there is few satisfying precision

grinding models for engineering applications and less theory to explain the grinding issues of micro-diameter optical crystal materials; thus, deep understanding is very necessary in the precision grinding technology, grinding ratio [7, 8], as well as the YAG optical crystal base material fabrication of the precision grinding process.

Model and approaches are significant for the grinding on a hard-brittle material, such as silicon and YAG. To characterize the whole grinding conditions, a novel model for the maximum undeformed chip thickness is proposed, and the calculated results are in good agreement with those of grinding on brittle materials [9, 10]. To investigate the grinding mechanisms of a hard-brittle material, traditional scratching using a single grain is employed from $\mu\text{m/s}$ to mm/s , which is three to six orders of magnitude lower than pragmatic machining of m/s [11].

To overcome this challenge, a novel approach of single grain scratching is suggested at nanoscale depth of cut and 40.2 m/s , which is four to seven orders of magnitude higher than the speeds used in conventional single grain scratching [12]. Force, stress, depth of cut, and size of plastic deformation are calculated at both onsets of chip formation and brittle-to-ductile transition for a hard-brittle material [13]. Under the breakthrough of theories, novel diamond wheels and grinding approaches are developed [14, 15]. These studies are a great contribution to the conventional grinding and manufacturing [16].

Centerless grinding is a kind of high precision grinding manufacturing process, which its widely applied to the aerospace and optical fields. However, the processing of optical crystal materials such as YAG with the microcylindrical diameter has a great influence on the roundness and parallelism of the workpiece [17]. So far, not much effective process have been proposed in engineering application background to flat and blunt grinding edges [18] and to solve the problem of roundness and parallelism of the workpiece processed by the YAG raw material.

In this paper, we propose a new process for grinding optical crystal materials by face-face precision grinding is developed. Based on the centreless grinding process fabrication the YAG optical crystal with grinding process function system that is designed. The ceramic base condition is further analyzed by regulating wheel axis experimental parameters, controllable clearance, and eccentricity for the e .

2 The experimental principle and process

The two ceramic grinding wheels do not rotate with constant speed, and the dressing wheel for a tiny feed speed leads to insufficient precision grinding of the final surface topography of the grinding wheel. Tiny abrasive particles with tiny speed cannot form the sharp multiple-tiny-grinding edges. In contrast, the block sharpening process is much more functional [19, 20]. The rotating speed of ceramic grinding wheel keeps constant during the precision grinding and

self-adaption-dressing process to avoid the deviation caused by centrifugal force.

Figure 1 shows the ceramic-based grinding wheels face-face for precision grinding design with the 3D design model of the assembly and the self-finishing wheel axis and C45 (the professional term for mechanical processing) for the 45° chamfering microprocess of the precision centerless grinding.

The design approach of the centerless grinding parameter design with ceramic base grinding wheel precision grinding can provide the precision grinding process region [21, 22]. The difficulty of the advancing precision grinding technology to process YAG optical crystal material finish surface is to resolve the mains parameters for the chamfering auxiliary tool design of the ceramic base grinding wheel. Through the chamfering auxiliary tool design and the mathematical geometry calculation, the design results show the conventional microprocess as shown in Figs. 1 and 2.

In grinding and precision grinding process of the cylindricity, parallelism and thermal damage are the key research topics. The change in tilt is related to the cylindricity and parallelism in tangential and normal directions region changes (the parameter adjustment, as shown in Tables 1 and 2 and Figs. 3 and 4).

For the Δa_p , it is necessary to be designed and calculated by the dynamic precision and ultra-precision grinding process. In general, “dressing tool accuracy” determines the finish surface accuracy of the grinding wheel. Moreover, the relative rotation velocity and the direction of the linear velocity of rotation affect the a_p precision grinding depth in the YAG optical crystals material processing. During the precision grinding error compensation, the grinding edge of the grinding wheel may generate a tiny amount of grinding mechanothermal model [23, 24].

Considering that the finish-surface thermal damage during precision grinding process affects the surface quality

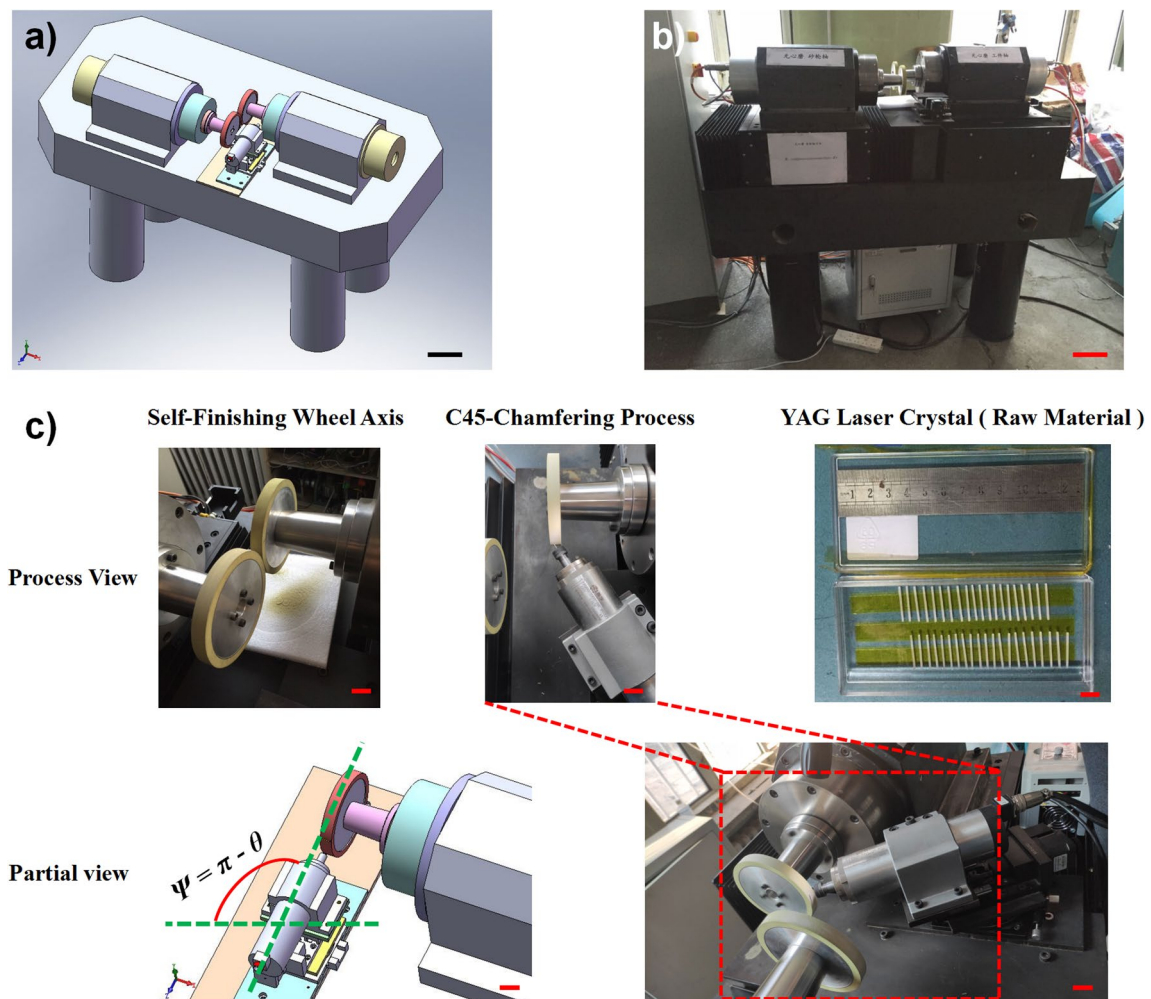


Fig. 1 Ceramic-based grinding wheels face-face for precision grinding design: **a**, **b** with the 3D design model assembly and **c** with self-finishing wheel axis and C45 for the chamfering process of the precision centerless grinding

Fig. 2 In the real-time precision grinding process area of the ceramic base grinding wheel along X+ and X- directions: **a** with the ceramic base grinding wheel and **b** 3D assembly model of the precision grinding wheel

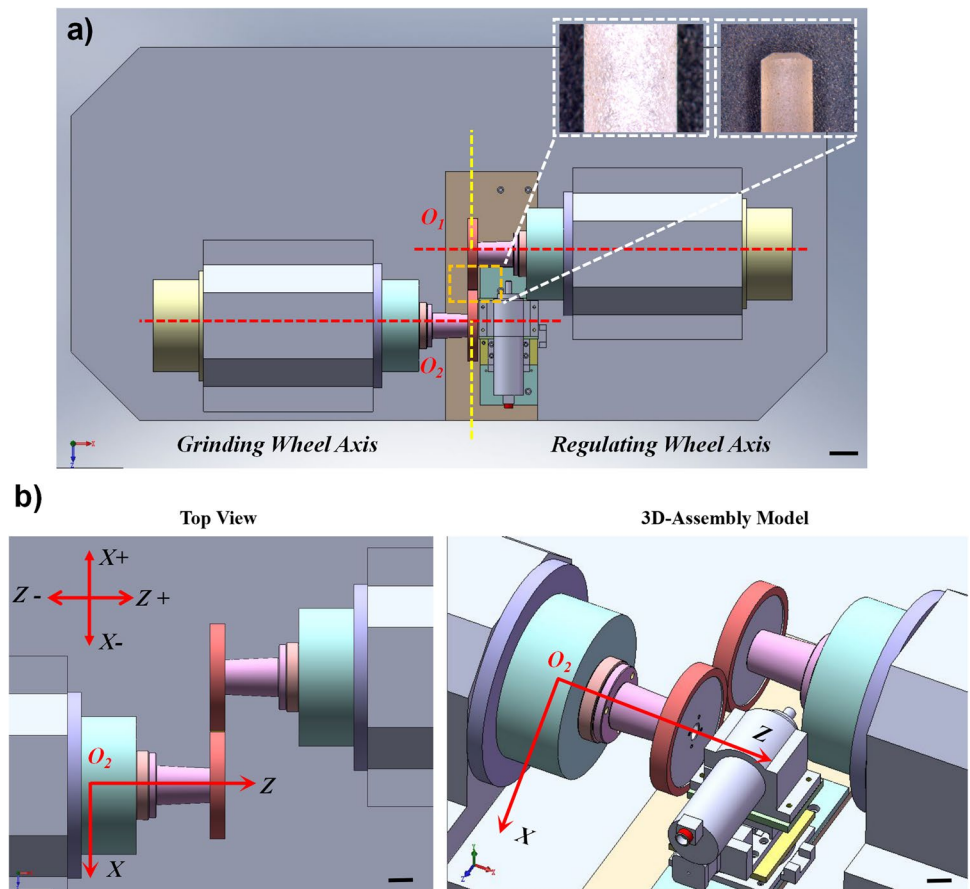


Table 1 Wheel and guide axis speed for the YAG grinding area location region

Grinding wheel axis speed (RPM)	Regulating wheel axis speed (RPM)	Turning around (-/-)	Feed location region ($\mu\text{m/s}$, direct influence a_p)	Gap and error range (μm)	Error range (μm)	Feed rate ($\mu\text{m/s}$)	Round beating noise (trend)
35	35.02	G-, R-	[0.022, 1.007]	0.9	± 0.016	0.8	↓
45	45.02	G-, R-	[0.022, 1.007]	0.9	± 0.014	0.8	→
50	50.02	G-, R-	[0.022, 1.007]	0.9	± 0.012	0.8	→
55	55.02	G-, R-	[0.022, 1.007]	0.9	± 0.012	0.8	↑
60	60.02	G-, R-	[0.022, 1.007]	0.9	± 0.012	0.8	↑

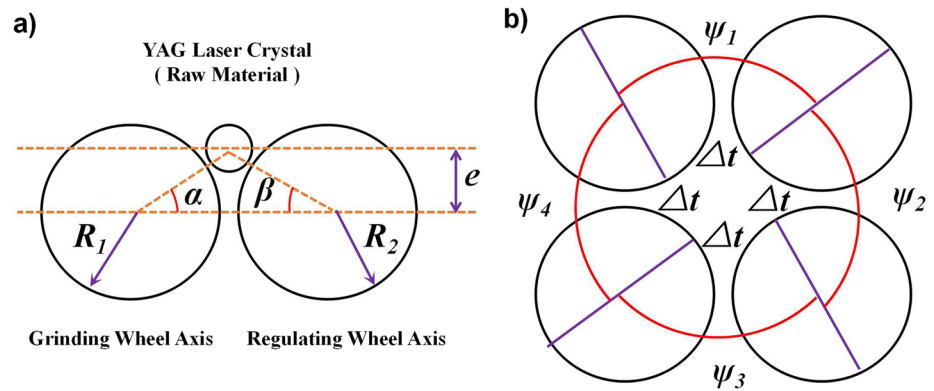
G- represents the “grinding wheel axis speed” is -, counterclockwise rotation; R-, represents the “regulating wheel axis speed” is -, counterclockwise rotation

Table 2 Feed location region for the regulating wheel axis and electric spindle

Regulating wheel axis speed (RPM)	Electric spindle speed (RPM)	Guide axis (-/-)	Feed location region ($\mu\text{m/s}$, direct influence a_p)	Electric spindle parameter adjustment	Error range ($^\circ$)
200	120	G-	[0.022, 1.007]*	25°	± 0.015
350	80	G-	[0.022, 1.007]	30°	± 0.015
500	75	G-	[0.022, 1.007]	35°	± 0.015
600	50	G-	[0.022, 1.007]	45°	± 0.015
670	30	G-	[0.022, 1.007]	50°	± 0.015

*G-, represents the “Grinding Wheel Axis Speed” is -; [a, b] indicates the maximum and minimum values of the “Feed Location Region”

Fig. 3 In the precision center-less grinding process of the grinding wheel axis and regulating wheel axis: **a** grinding rotation angle and the eccentricity of e ; **b** direction of rotation of the Ψ ; **c** scatter matrix



c)

	x_1	x_2
	Scatter Matrix	
	Grinding Wheel Axis Speed	Regulating Wheel Axis Speed
Grinding Wheel Axis Speed	G^-	G^-, R^+
Regulating Wheel Axis Speed	G^-, R^+	R^+

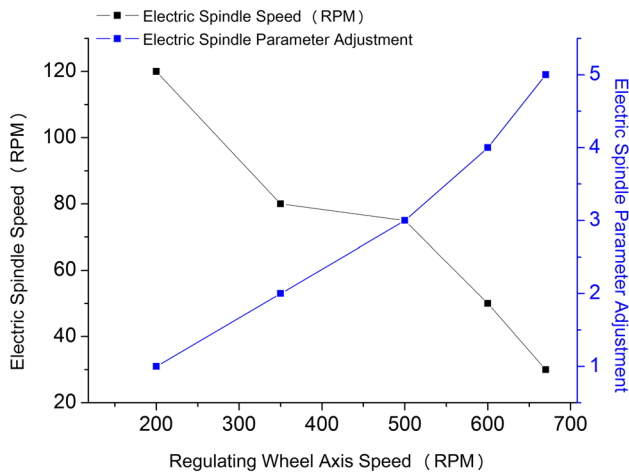


Fig. 4 In precision grinding process of the feed location region ($\mu\text{m/s}$, direct influence a_p) with the parameter relationship between the regulating wheel axis speed and the electric spindle speed

and optical properties of the YAG optical crystals, it is possible to immerse the YAG workpiece in the ethanol and alcohol ($\text{C}_2\text{H}_5\text{OH}$, or $\text{CH}_3\text{CH}_2\text{OH}$) that works as a “coolant” before grinding. On the one hand, it provides a cooling effect and prevents heat accumulation; on the other hand, alcohol is easy to volatilize, therefore not affecting the optical properties of the YAG optical crystals by the

workpiece (room temperature, as shown in Fig. S2 of the Appendix A. Supplementary data).

In order to suppress the thermal damage to the surface quality of the YAG optical crystal samples, an appropriate amount of ethanol and alcohol was used for immersion, which additionally improves the efficiency of precision grinding and reduces the effect of sharpening of tiny particles on the finish surface quality of grinding process. This method is simple and feasible. By real-time adjusting the speed of the ceramic-based grinding wheel according to the eccentricity e created from the gap between the grinding wheel and regulating wheel, stable precision grinding parameters are obtained. The grinding diameter of YAG optical crystal workpiece is controlled in a range between 0.35 and 0.9 mm (<1 mm), the YAG ($\text{Y}_3\text{Al}_5\text{O}_{12}$) optical property parameters as shown in Table S1 and the microgrinding results as shown in Fig. S2 of the Appendix A. Supplementary data.

For the ceramic-based grinding wheel, a more effective grinding wheel self-adaption-dressing process is presented. Based on the affiliated relationship between the material removal rate and the ceramic grinding wheel morphology during the grinding wheel sharpening process, the surface peak value is eliminated through “the grinding of the face-face” process to achieve smooth working condition. In the process of ceramic base grinding wheel self-adaption dressing, the critical parameters are controlled by adjusting the rotation direction, i.e., grinding wheel axis (-) or the

regulating wheel axis (-) to determine the final appearance of the grinding wheel, as shown in the Table 1 and Fig. 3.

The solution in this paper is to apply YAG microdi- ameter optical crystals to the precision grinding process, which is known to be prepared functional optical crystal materials with a diameter < 1 mm. The gap and error range show that the law of decreasing arithmetic sequence is $a_{n+1} \leq a_n$ ($n \in N$) and the YAG optical crystals of the precision grinding each decrease is 0.015 mm and finish diameter range is [0.3, 1.2]. For rotary process, ceramic-based grinding wheel is also a dressing tool in self-rotating correction technology. It is found that the speed ratio in the dressing process is $V_{grinding\ wheel} > V_{regulating\ wheel}$ and $V_{grinding\ wheel} \approx V_{regulating\ wheel} + 0.02$ (RPM, the grinding force and speed difference are formed), as shown in the Table 1.

In the centerless grinding process, the normal grinding force F_n , the speed ratio $V_{grinding\ wheel}$, and $V_{regulating\ wheel}$ mainly affect the finish surface quality. These factors directly affect the finish surface shape of the YAG optical crystals material. Therefore, we present the design with “the grinding of the face-face” process and calculation results and analyze the experimental principle and conditions of the parameters including the precision grinding ratio, self-rotating correction technology, and a_p . The mathematical analysis model of the shaping during finish surface grinding is described in Fig. 3 a and b.

The tangential acceleration in the tangential direction is maximized when the ceramic-based grinding wheel is contacted. The circular round to beat and parallelism at the touch-point depend on the relative precision of the two ceramic grinding wheels and the feed speed, as well as the grinding margin allowed to be removed.

Therefore, we propose a method of grinding wheel dress- ing, in which two ceramic grinding wheels (both the grind- ing wheel and regulating wheel) are grinding face-face to achieve dressing the grinding wheel. The beating amount of the YAG optical crystal with the finish surface errors are removed by the margin of the face-face precision grinding process. The finish touch surface of the ceramic grinding wheel has a high grinding quality of cylindricity and paral- lelism and a tiny effective roughness with tiny grinding particles that form tiny grinding touch edges. It is noted that improper adjustment parameters lead to continuous changes in the grinding force and slight pulsation and accordingly less smooth and densification of the surface finish quality.

3 Microgrinding force calculation analytic and discussion

For centerless grinding processes, finish surface thermal damage and microgrinding force includes the amount of micro-jumping and friction during grinding process. The

grinding deformation force includes the grinding tangen- tial forces and normal forces along the centerless grinding direction of rotation. When the angle of the ceramic-based grinding wheel axis and regulating wheel axis is 2θ , the mathematical model formula of the centerless grinding force can be described as the slight elastic deformation and bal- ance equation:

$$\begin{cases} F_{grinding\ wheel} \cdot \cos \theta + F_{regulating\ wheel} \cdot \cos \theta = F_g + F'_t \cos \psi, F_n = \left| \sum_{i=1}^n \vec{f}_0 \right| \\ F_{grinding\ wheel} \cdot \sin \theta + F'_t \sin \psi = F_{regulating\ wheel} \cdot \sin \theta \\ M = F'_t \cdot \left(\frac{D_{YAG}}{2} - \delta_{YAG} \right) = (F_{regulating\ wheel} - F_{grinding\ wheel}) \cdot \frac{D_{YAG}}{2} \end{cases} \quad (1)$$

If the speed difference between the two ceramic-based grinding wheels is not appropriate, the YAG optical crystal will be slightly beaten. Along the tangential direction of the grinding profile, the YAG workpiece is subjected to a tan- gential grinding force F , and the equilibrium force equation is as follows:

$$\begin{cases} F_N = F_n, F_T + F_t \\ M = F_n \cdot L(t) \end{cases} \quad (2)$$

With this design, the grinding efficiency of the YAG opti- cal crystal is improved by 80%, as shown in Table 1.

3.1 Grinding ratio and force calculus method

At room temperature, the model parameters of grinding wheel axis and regulating wheel axis directly affect a_p of the grinding depth. If the ceramic-based grinding wheel axis speed and regulating wheel axis speed (RPM) of the YAG laser crystal are considered a whole system, a slight bending moment M will be generated along the normal direction of the grinding profile to downward positive pressure. The G- (represent the “grinding wheel axis speed” is -) and R- (the “regulating wheel axis speed” is -) are shown in Table 1 and the scatter matrix in Fig. 3.

Figure 4 shows the parameter relationship between the regulating wheel axis speed and the electric spindle speed in precision grinding process of the feed location region. The workpiece of YAG optical crystal is a solid cylinder, and the axial stress created is uniform (diameter D /cylinder length L is very small). If the resultant force of the external force passes through the grinding wheel axis, the cross-section is only subjected to tensile stress. The normal stress and shear stress exist on a section at an angle to the axis, and the values are a function of the angle between the normal of the section and the axis.

The influence of the rotational precision grind- ing amount is obtained by a mathematical calculation model of YAG laser crystal finish surface forming pro- cess with L/D ratio. And the results are then verified by

experimental tests under the condition of precision grinding technology (as shown in Euler’s formulas (2–5)).

When the ratio of length/L to diameter/D satisfies $L/D \leq M$ condition, the critical surface pressure of YAG cylindrical workpiece can be calculated by Euler’s formula:

$$\lambda = \frac{\mu l}{i} \tag{3}$$

$$\sigma_{cr} = \frac{\pi^2 E}{\lambda^2} \tag{4}$$

At that time, the precision grinding trajectory equation is the hyperbolic form of the Euler’s curve as shown below:

$$Euler's\ Hyperbolic_{YAG} = \frac{\pi^2 E}{(L/D)^2} \tag{5}$$

where M is the torque; L the length of the YAG optical crystal; D the diameter of the YAG optical crystal; E stress intensity; and π is 3.1415926.

Here, we take into account of the precision grinding processes of the processing errors in the accomplish types of the microscale chamfering (YAG raw materials, as shown in Fig. S2a).

According to the stress strength of the material and the diameter of the precision grinding (< 1 mm), the wheel speed and steering (counterclockwise and clockwise) make the precisely adjusted, which the diameter of the optical crystal material make the accurately grinding to less than 1 mm quickly. Euler’s formula was be used to calculate the curve trajectory of optical crystal materials and the centrifugal distance and eccentric distance parameter e (Formula 8) based on centerless precision grinding process quickly before precision grinding.

Of course, the disadvantage of this work is that the grinding wheel’s outer circle parameters need to be trimmed timely according to the grinding wheel’s precision grinding wear degree. Once the grinding wheel collapses locally and the two grinding wheels rotate at the same speed (clockwise or counterclockwise at the same time), the optical crystal material will directly collapse, fracture, and crack.

Where α and β are the rotation characteristic parameters of the normal and tangential directions of the process of YAG optical crystal grinding when one-part deviates from the center of the grinding wheel, the balance equation of the tangent point position on the workpiece touch surface is:

$$\alpha = \arccos \left[\frac{R_{YAG}^2 - r_e^2 + R_{o_1/o_2}^2}{2R_{YAG}R_{o_1/o_2}} \right] \tag{6}$$

$$\beta = \arccos \left[\frac{R_{YAG}^2 - r_e^2 + R_{o_1/o_2}^2}{2R_{YAG}R_e} \right] \tag{7}$$

The touch point in precision grinding process is the force point of the tangent normal direction, and the paths of the rotation to beat parameter ω_1 and ω_2 are rotation characteristic parameters or characteristic parameters of rotation (RCP).

In this article, we give the eccentric distance parameter e is calculated as follows:

$$e = \left(\sqrt{(R_{Grinding\ Wheel} + R_{Regulating\ Wheel}) - e_{YAG}^2 - R_{Grinding\ Wheel} - Z} \right) \tan \beta + e_{YAG} - \frac{R_{Regulating\ Wheel}}{\cos \beta} \tag{8}$$

where R_{YAG} is the radius of the YAG optical crystal and e is the eccentric distance.

In order to design and calculate the adjustable parameterization of grinding clearance, it is necessary to establish an appropriate geometric model. The established grinding clearance is a coordinate system that describes the key parameters, design, and simulation of the entire assembly precision grinding process system, as shown in Fig. 3 a and b.

According to the experimental conditions, we observed that the abrasive particles of YAG laser crystal samples are worn and fell off during the process of precision grinding. Therefore, the grinding conditions in the precision grinding process of the centerless process are adjusted in real time, rather than keeping it constant. In a certain moment of precision grinding, the friction force can complete the precision grinding of the workpiece by the raw materials. However, along with this condition, the work finish surface quality is burned which causes potential damage.

3.2 The grinding force: the grinding ratio of e_s

Based on the stable rotation of the ceramic-based grinding wheel (both the grinding wheel and regulating wheel), the free vibration period is obtained in the precise grinding process of the YAG optical crystal, and the active damping system is realized. The higher feed speed and working speed created under the condition of no chatter are obtained as well. The normal and tangential forces and the grinding ratio with the coordinate system of the $O_1 (Z_1, X_1)$ and $O_2 (Z_2, X_2)$ can be calculated and created with the differential calculation by Eqs. (9)–(12).

According to Furukawa et al., $r_w (\Psi)$ is the rotation angle Ψ of the grinding touch contact point:

$$\varepsilon = \frac{\sin \psi_2}{\sin (\psi_2 - \psi_1)}, (1 - \varepsilon) = \frac{\sin \psi_1}{\sin (\psi_2 - \psi_1)} \tag{9}$$

Defining W_{YAG} as the angular angle of the YAG optical crystal, then

$$t = \frac{\psi_1}{\psi_{YAG}}, t = \frac{\psi_2}{\psi_{YAG}} \tag{10}$$

$$r_w(\psi) = \epsilon' r_w(\psi - \psi_1) - (1 - \epsilon) r_w(\psi - \psi_2) \rightarrow r_w(t) = \epsilon' r_w(t - t_1) - (1 - \epsilon) r_w(t - t_2) \tag{11}$$

It has been considered to grind surface quality; the grinding ratio with error compensation and a_p are considered during the YAG optical crystal (raw materials) precision grinding process. The grinding wheel axis speed and regulating wheel axis speed (RPM) create a speed discrepancy with the 0.02 mm (such as G-, R-, as shown in Table 1 and Fig. 3). The centerless grinding speed can be counterbalanced by calculating the normal and tangential forces and the grinding ratio:

$$e_s = \frac{E_{YAG}}{V_{grinding\ wheel}} = \frac{F_t}{V_{grinding\ wheel}} v_s = \frac{F_n}{V_{grinding\ wheel}} v_s [J/mm^3] \tag{12}$$

When the ceramic-based grinding wheel contacts with the YAG optical crystal, it produces rotational resistance, as shown in Fig. 6 (c) and Fig. 6 (d). The thrust in the normal direction increases the normal force of the abrasive particles. The force on the abrasive grain is shown in Fig. 4. Through extensive experiments of the precision grinding process, the error on the grinding ratio is e_s , as shown in Fig. 5.

Also, the ceramic-based grinding force mathematical model formula is as follows:

$$dF_s = F_i dA \cos \theta \cos \psi \tag{13}$$

where F_i is the grinding force per unit area (N/mm^2) and dA the actual contact area during the grinding process.

3.3 Characterization of Grinding depth a_p

The calculation method of rotation speed of YAG by the optical crystal cylindrical workpiece is shown below (Fig. 6):

$$\omega = \psi_i / \Delta t \tag{14}$$

where ψ_i is the rotation angle and Δt , the rotation interval time.

The equilibrium equation for uniform rotation [25, 26] is as follows:

$$\Omega_s = 2V_{grinding\ wheel} / D_{YAG} \tag{15}$$

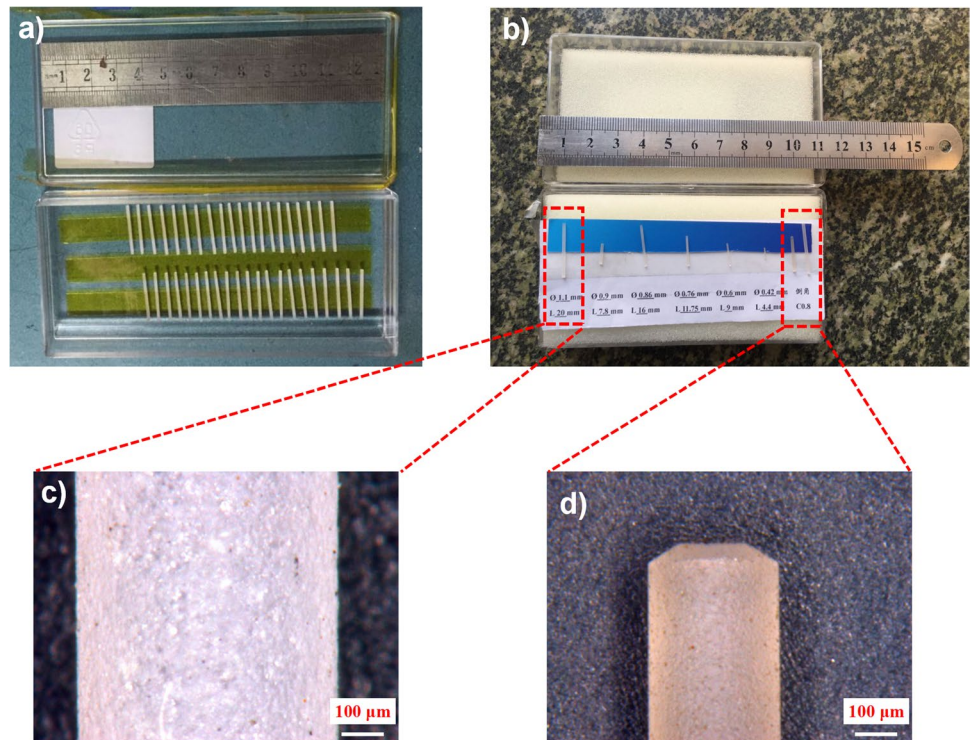
where Ω_s is constant speed, $V_{grinding\ wheel}$ the ceramic-based grinding wheel, and D_{YAG} the diameter of the YAG optical crystal.

Also, the diameter of the YAG optical crystal is 1.2 mm or 1.4 mm (raw materials, as shown in Fig. 6a).

Therefore, the precision grinding of the tangent and normal force density function is as follows:

$$df(\psi) = g_d(\beta) f_{grinding\ wheel}(\theta) d\theta \tag{16}$$

Fig. 5 The grinding results: **a, b** the YAG laser crystal raw material; **c, d** the precision grinding of functional materials with microdiameter laser crystals < 1 mm



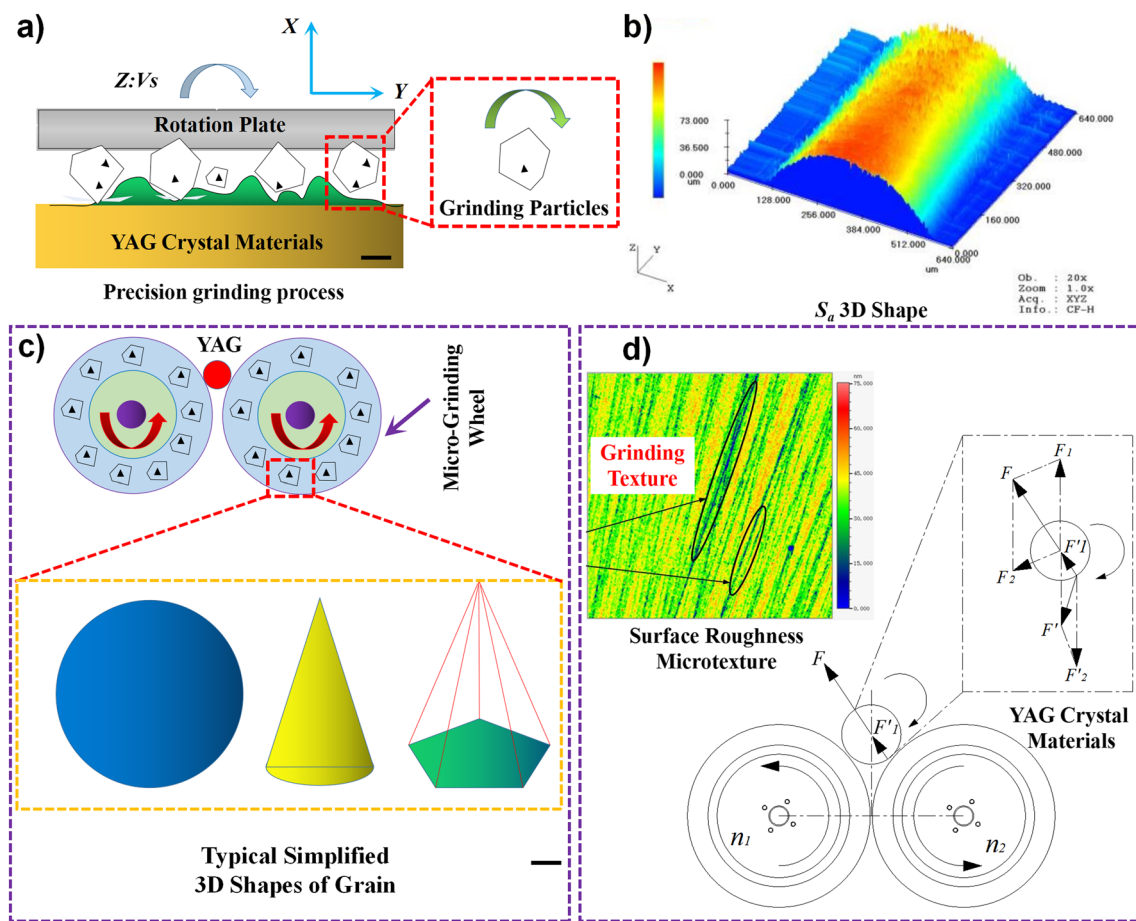


Fig. 6 The 3D microtexture test results: **a** precision grinding process; **b** 3D/three-dimensional shape of S_a ; **c** typical simplified 3D shapes of grain; **d** surface roughness microtexture and precision grinding force analysis diagram

The component of the grinding force in the Cartesian coordinate system can be described as the three-dimensional structure of the component [27, 28] in $ZX-\theta$ coordinate:

$$f_{grinding\ wheel} = \begin{Bmatrix} f_{gx}(\theta) \\ f_{gy}(\theta) \end{Bmatrix} = \begin{bmatrix} \cos \theta & \sin \theta \\ \sin \theta & -\cos \theta \end{bmatrix} \begin{Bmatrix} f_{gr}(\theta) \\ f_{gr}(\theta) \end{Bmatrix} \tag{17}$$

where $f_{grinding\ wheel}$ is the tangent and normal of the grinding force supply with the $ZX-\theta$ coordinate by the density function.

In the mathematical model, the tangential F_t and normal force F_n and per unit of the precision grinding width [29] and grinding depth a_p can be determined as follows:

$$\begin{cases} F_{tc} = \sum \phi Fenc = \phi K \sum Qi = \phi K \frac{Vw}{V_{grinding\ wheel}} a_p \\ F'_{tc} = K' \frac{Vw}{V_{grinding\ wheel}} a_p \\ K' = \phi K \end{cases} \tag{18}$$

The lower limit of the integral is θ , the upper limit is $\pi/2$, so:

$$S = 2\pi R \cdot R(1 - \sin \theta) \tag{19}$$

The mapping relationship in the 3D-Cartesian's coordinate system of the sphere (R, θ, Ψ) and the rectangular coordinate system (X, Y, Z) are as follows:

$$\begin{aligned} X &= R \sin \theta \cos \psi \\ Y &= R \sin \theta \sin \psi \\ Z &= R \cos \theta \end{aligned} \tag{20}$$

Hypothesis: The two ceramic grinding wheels (both the grinding wheel and regulating wheel) process of the rotational motion are uniform in the Cartesian's coordinate system. The equation of polar coordinates is as follows:

$$\Gamma : X = \rho \cos \theta, Y = \rho \sin \theta, Z = k\theta, 0 \leq \theta \leq 2\pi \tag{21}$$

In the precision grinding process of optical crystal and optically difficult-to-grinding materials, it is related to k , but it is necessary to control the precision grinding gap between two ceramic-based wheels (room temperature, as shown in Table 1, Fig. 6, and Fig. S2).

In the Cartesian's coordinate system, the mapping relation of along the base and the tangent direction are as follows:

$$\begin{cases} dL(R) = dR \\ dL(\psi) = R \sin \theta d\psi \\ dL(\theta) = Rd\theta \end{cases} \quad (22)$$

In the precision grinding process of the ceramic base grinding wheel, the grinding ability of the grinding wheel's tiny abrasive particles determines the "grinding ratio" and "grinding depth of the a_p " in the face-face precision grinding process. The depth of the feed of the a_p is defined by functions as follows:

$$L_{\text{hypotenuse}} = \frac{N_{\text{dividing plate}}}{360} \times P_{\text{screw pitch}} \quad (23)$$

$$\sin \theta = \frac{L_{\text{opposite side}}}{L_{\text{hypotenuse}}} = \frac{a_p}{L_{\text{hypotenuse}}} \quad (24)$$

where $N_{\text{dividing plate}}$ is the number of teeth of indexing dial and $P_{\text{screw pitch}}$ is the pitch of the feed direction.

Additionally, the cylindricity and parallelism of ceramic-based grinding wheel by the dressing directly affect the surface finish quality of YAG optical crystal and the accuracy of precision grinding.

Based on the precision grinding process of two centerless grinding wheels, the grinding force increases with the increase of cutting depth, and the crack depth should also increase according to the knowledge of linear elastic fracture mechanics. At the edge of optical crystal material, the phenomenon of workpiece edge breakage is more serious.

4 Ceramic wheel grinding force analysis of the particle size result

For chamfering process of the electric spindle: (1) The greater the swing angle, the lower the speed; (2) the smaller the swing angle, the higher the speed. For chamfering process of the regulating wheel axis: (1) The greater the swing angle, the higher the speed; (2) the smaller the swing angle, the lower the speed (room temperature, as shown in Table 2 and Fig. 4).

Figure 5 shows the grinding region for the grinding wheel axis and regulating wheel axis of the typical simplified shapes of grain and the grinding direction. Figure 6 shows the 3D (three-dimensional) shape microtexture test results of S_a , surface roughness microtexture and precision grinding force analysis diagram. Figure 7 indicates the YAG optical crystal material particle sizes of the YAG optical crystal raw material, as well as a histogram graph of the axial direction and radial direction grinding region trend increase chart.

Based on the centerless precision process, the edge of the microdiameter laser crystal with a diameter of less than 1 mm does not collapse and fracture. When the precision grinding direction is clockwise or counterclockwise at the same time, the grinding results are consistent. For the chamfer of a small diameter cylinder (< 1 mm), no fracture occurs.

The workpiece diameter is relatively small (< 1 mm) and cannot be measured by traditional methods such as cylindricity meter. We propose a laser confocal microscope to scan the cylindrical surface of workpiece and record the position of coordinates on each point. The principle of calculating cylindricity error of precision grinding YAG crystal material is to take the maximum roundness error measured

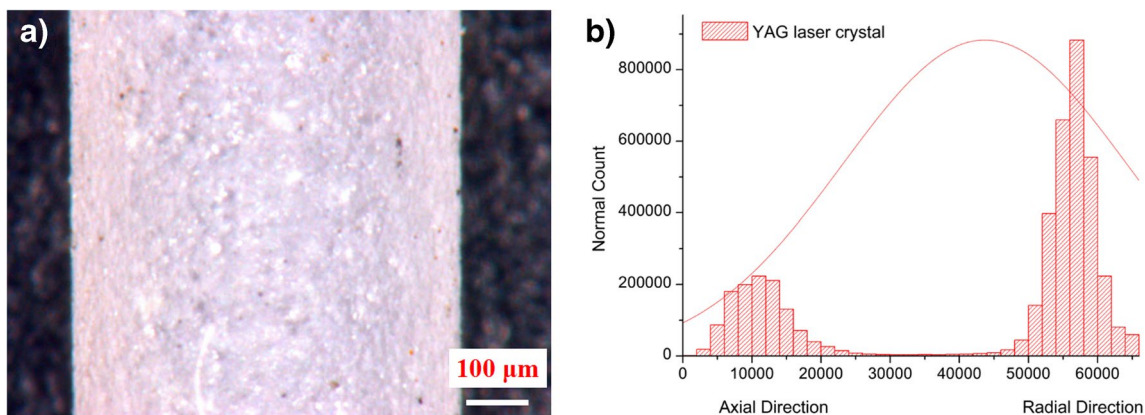


Fig. 7 Plot the numerical value of the YAG optical crystal material particle sizes result: **a** the YAG optical crystal material of the raw material; **b** a histogram graph of the axial direction and radial direction grinding region trend increase chart

by different cross sections and the maximum straightness error measured by each prime line. The calculation method is according to the theoretical calculation formulas (25–26). The $f_{cylindricity}$ is defined by functions as follows:

$$f_{cylindricity} = f_{circular\ degree(max)} + \frac{1}{2}f_{parallelism(max)} \quad (25)$$

$$f_{cylindricity} = f_{straightness(max)} + \frac{1}{2}f_{circular\ degree(max)} \quad (26)$$

where $f_{cylindricity}$ is the 3D cylindricity error of workpiece surface.

In addition, the grinding feed for a_p affects surface grinding quality of the YAG optical crystal material of the two ceramic grinding wheels (both the grinding wheel and regulating wheel), which are grinding of the face-face to achieve dressing the grinding wheel with the chamfering auxiliary device by the calculus of the precision grinding (as shown in Fig. S1 of the “Appendix A. Supplementary data”).

Figure S2 illustrates the grinding results of the YAG optical crystal raw material and the precision grinding of functional materials with microdiameter optical crystals by the precision grinding process results. For the other mains and key of the results and parameters, such as the grinding ratio for centerless microgrinding with the grinding surface finish quality of the YAG optical crystal, please refer to the supporting materials in the “Appendix A. Supplementary data” with Fig. S2.

5 Conclusions

This paper presents a centerless grinding of the YAG optical crystal grinding process; we design a mathematical model and precision process which are supported as an effective process to control over the YAG optical crystal surface finish and grinding accuracy. For the centerless grinding process (both the grinding wheel axis and regulating wheel axis), the grinding process works at the RT of $25 \pm 1.5^\circ\text{C}$ (room temperature), and the grinding ratio relation e between grinding ratio and the centerless grinding depth a_p controls the precision grinding amount during the YAG optical crystal surface finish grinding process.

The work illustrates the selection of an appropriate and optimal self-adaption dressing process for the grinding wheel parameters, which are of significance to the finish surface quality, cylindricity, and parallelism of the ceramic base grinding wheel in precision grinding. From the analysis of the precision grinding process, it provides a profound insights into the grinding ratio e_s and the complex grinding of microdiameter optical crystal raw materials. In the scenario of “test micro-speed,” the rotation speed of the two ceramic base grinding wheels (both the grinding wheel and regulating wheel) can be set as stable or unstable, and the

linear velocity in the direction of rotation is always opposite (G-, R-), as shown in Table 1 and Fig. 3.

The YAG optical crystal surface finish fabrication and precision grinding process has been proved to be a targeted control method for solving the grinding ratio, cylindrical, and parallelism of the YAG optical crystal. This paper study the accuracy with the two ceramic grinding wheels (both the grinding wheel and regulating wheel) via the grinding ratio and a_p . The main conclusions are summarized as follows:

- (1) Based on centerless precision grinding process, the value range of the feed location region is [0.022, 1.007]. Grinding wheel axis speed and regulating wheel axis speed are 35~60 RPM.
- (2) The feasibility of self-adaption-dressing process for centerless grinding is verified. To improve the finish surface quality, roundness and parallelism of the YAG optical crystal are established in the geometric mathematical model which is then tested in verification.
- (3) A 3D (three-dimensional) analytical model and precision process for the precise centerless grinding of YAG crystal material is established. Microgrinding gap geometry and precision grinding process parameters based on real-time adjustment are designed and tested.

Supplementary Information The online version contains supplementary material available at <https://doi.org/10.1007/s00170-023-12193-4>.

Acknowledgements The authors wish to express gratitude for the generous support from Laboratory of Optical System Advance Manufacturing Technology, Changchun Institute of Optics, Fine Mechanics and Physics (CIOMP), Chinese Academy of Science researchers. Also, we wish to thank Dianrong Luan for grinding process, who devoted for the precision machinery offering senior expert and senior technician from Harbin Institute of Technology. The original process idea is designed by Jiabin Xu, a Ph.D. candidate under the guide from Prof. Feihu Zhang.

Author contribution All authors contributed to the study conception and design. Material preparation, data collection, and analysis were performed by Jiabin Xu. The first draft of the manuscript was written by Jiabin Xu, and all authors commented on previous versions of the manuscript. Jiabin Xu and Qiongyi He contributed equally to this work and should be considered co-first authors. The grinding opinion in the invention patent shall be modified and improved by Qiongyi He, Xiangyu Zhang, Yang Yu, and Dongyu Tian. This work was supported by Feihu Zhang (Grant No. 2016YFB1102204 and Grant No. 2018ZX04015001-005). All authors read and approved the final manuscript.

Funding This work was funded and financial support by the National Key R&D Program of China (Grant No. 2016YFB1102204) and the National Science and Technology Major Project of the Ministry of Science and Technology of China (Grant No. 2018ZX04015001-005).

Data availability No applicable.

Code availability The concepts of coding were presented with pseudocode in the article; thus, there is no access for the custom code. No applicable.

Declarations

Ethical approval The research does not involve human participants and/or animals.

Informed consent Consent to submit the paper for publication has been received explicitly from all co-authors.

Competing interests The authors declare no competing interests.

References

- Hashimoto F, Lahoti G.D (2004) Optimization of set-up conditions for stability of the centerless grinding process. *Annals of the CIRP* 53(1), pp.271–274
- Mannan MA, Drew SJ, Stone BJ (2002) Torsional vibration effects in grinding. *CIRP Annals* 49(1):249–252
- Qi B, Yu S, Yong B, Qin-Jun P, Zu-Yan X (2021) Study on properties of Nd:YAG ceramic microchips with different concentration. *Opt Mater* 120:111425
- Quang NM, Tung NT, Thanh LTP (2022) Study of the polishing performance of yag crystals through the balance between chemical and mechanical actions. *J Inst Eng India Ser C* 103:1223–1233
- Barrenetxea D, Marquinez JI, Bediaga I (2009) Continuous work-piece speed variation (CWSV): Model based practical application to avoid chatter in grinding. *CIRP Ann Manuf Technol* 58(1):319–322
- Ma L, Li M, Komasa S, Yan S, Yang Y, Nishizaki M, Chen L, Zeng Y, Wang X, Yamamoto E, Hontsu S, Hashimoto Y, Okazaki J (2022) Characterization of hydroxyapatite film obtained by Er:YAG pulsed laser deposition on sandblasted titanium: an in vitro study. *Materials* 15(6):2306
- Chen F, Mei G, Zhao B (2020) Study on the characteristics of zirconia ceramic in three-dimensional ultrasonic vibration-assisted ELID internal grinding. *J Mech Sci Technol* 34(1):333–344
- Ahrens M, Dagen M, Denkena B, Ortmaier T (2016) An active damping method for chatter vibration in plunge grinding using electromagnetic actuators. *Procedia CIRP* 46:197–200
- Inasaki I, Karpuschewski B, Lee H-S (2001) Grinding chatter-origin and suppression. *CIRP Annals* 50(2):515–534
- Zhenyu Z, Fengwei H, Xianzhong Z, Dongming G (2012) Fabrication and size prediction of crystalline nanoparticles of silicon induced by nanogrinding with ultrafine diamond grits. *Scr Mater* 67(7–8):657–660
- Zhenyu Z, Yaxing S, Chaoge X, Dongming G (2012) A novel model for undeformed nanometer chips of soft-brittle HgCdTe films induced by ultrafine diamond grits. *Scr Mater* 67(2):197–200
- Zhenyu Z, Dongming G, Bo W, Renke K, Bi Z (2015) A novel approach of high speed scratching on silicon wafers at nanoscale depths of cut. *Sci Rep* 5:16395
- Zhenyu Z, Bo W, Renke K, Bi Z, Dongming G (2015) Changes in surface layer of silicon wafers from diamond scratching. *CIRP Annals* 64(1):349–352
- Zhenyu Z, Xin W, Fanning M, Dongdong L, Siling H, Junfeng C, Jianmei W, Wei W (2022) Origin and evolution of a crack in silicon induced by a single grain grinding. *J Manuf Process* 75:617–626
- Zhenyu Z, Junfeng C, Bo W, Ziguang W, Renke K, Dongming G (2017) A novel approach of mechanical chemical grinding. *J Alloys Compd* 726(5):514–524
- Zhang Z, Huang S, Wang S et al (2017) A novel approach of high-performance grinding using developed diamond wheels. *Int J Adv Manuf Technol* 91:3315–3326
- Bo W, Zhenyu Z, Keke C, Junfeng C, Rosenkranz A, Jinhong Y, Lin C-T, Chen G, Ketao Z, Jun L, Nan J, Dongming G (2018) New deformation-induced nanostructure in silicon. *Nano Lett* 18(7):4611–4617
- Derkx JM (2008) High precision form crush profiling of diamond grinding wheels. Technische Universiteit Delft, Delft
- Salje E, Scharfen HU (1990) *Kunstharzgebundener CBN-Profileschleifscheiben mit Korundblock und mit Strahl*, Jahrbuch Schleifen, Honen, Lappen und Polieren 56:202–216
- Salje E (1990) Wirkungsweisen und Anwendungen von Konditionierverfahren. *CIRP Ann Manuf Technol* 39(1):337–340
- Rowe WB, Miyashita M, König W (2004) Centreless grinding research and its application in advanced manufacturing technology. *Annals of the CIRP* 38(2):617–625
- Klocke F, Friedrich D, Linke B, Nachmani Z (2004) Basics for in-process roundness error improvement by a functional workrest blade. *Annals of the CIRP* 53(1):275–280
- Hecker RL, Ramoneda IM, Liang Steven Y (2003) Analysis of wheel topography and grit force for grinding process modeling. *J Manuf Process* 5(1):13–23
- Kang RK, Yuan JT, Zhang YP, Ren JX (2001) Truing of diamond wheels by optical. *Key Eng Mater* 202–203:137–142
- Zhang H, Lieh J, Yen D, Song X, Rui X (2003) Geometry analysis and simulation in shoe centerless grinding. *J Manuf Sci Eng T ASME* 125:304–309
- Wu Y, Kondo T, Kato M (2005) A new centerless grinding technique using a surface grinder. *J Mater Process Technol* 162–163:709–717
- Wu Y, Fan Y, Kato M, Wang J, Syoji K, Kuriyagawa T (2003) A new centerless grinding technique without employing a regulating wheel. *Key Eng Mater* 238–239:355–360
- Chang HC, Wang J, Junz J (2008) A stochastic grinding force model considering random grit distribution. *Int J Mach Tool Manuf* 48(12–13):1335–1344
- Li L, Fu J (1980) A study of grinding force mathematical model. *Annals of CIRP-Manuf Technol* 29(1):245–249

Publisher's note Springer Nature remains neutral with regard to jurisdictional claims in published maps and institutional affiliations.

Springer Nature or its licensor (e.g. a society or other partner) holds exclusive rights to this article under a publishing agreement with the author(s) or other rightsholder(s); author self-archiving of the accepted manuscript version of this article is solely governed by the terms of such publishing agreement and applicable law.

Authors and Affiliations

Jiabin Xu¹  · Qiongyi He² · Xiangyu Zhang³ · Yang Yu² · Dongyu Tian¹ · Yingjie Li⁴ · Feihu Zhang¹

¹ School of Mechatronics Engineering, Aeronautics and Astronautics Manufacturing Engineering, Harbin Institute of Technology, Harbin, China

² School of Mechanical Engineering, Tianjin University of Technology and Education, Tianjin, China

³ CNC Engineering Training Center, Tianjin University of Technology and Education, Tianjin, China

⁴ Laboratory of Optical System Advance Manufacturing Technology, Changchun Institute of Optics, Fine Mechanics and Physics (CIOMP), Chinese Academy of Science, Changchun, China